Anisotropic Effective Mass, Optical Property and Enhanced Band Gap in BN/Phosphorene/BN Heterostructures

ARTICLE *in* ACS APPLIED MATERIALS & INTERFACES · OCTOBER 2015

Impact Factor: 6.72 · DOI: 10.1021/acsami.5b05694

2 AUTHORS, INCLUDING:

Tao Hu

Pukyong National University

10 PUBLICATIONS **51** CITATIONS

SEE PROFILE

ACS APPLIED MATERIALS & INTERFACES

Research Article

www.acsami.org

Anisotropic Effective Mass, Optical Property, and Enhanced Band Gap in BN/Phosphorene/BN Heterostructures

Tao Hu and Jisang Hong*

Department of Physics, Pukyong National University, Busan 608-737, Korea

ABSTRACT: Phosphorene is receiving great research interests because of its peculiar physical properties. Nonetheless, the phosphorus has a trouble of degradation due to oxidation. Hereby, we propose that the electrical and optical anisotropic properties can be preserved by encapsulating into hexagonal boron nitride (h-BN). We found that the h-BN contributed to enhancing the band gap of the phosphorene layer. Comparing the band gap of the pristine phosphorene layer, the band gap of the phosphorene/BN(1ML) system was enhanced by 0.15 eV. It was further enhanced by 0.31 eV in the BN(1ML)/phosphorene/BN(1ML) trilayer structure. However, the band gap was not further enhanced when we increased the thickness of the h-BN layers even up to 4 MLs. Interestingly, the anisotropic effective mass and optical property were still preserved in BN/phosphorene/BN heterostructures. Overall, we predict that the capping of phosphorene by the h-BN layers can be an excellent solution to protect the intrinsic properties of the phosphorene.

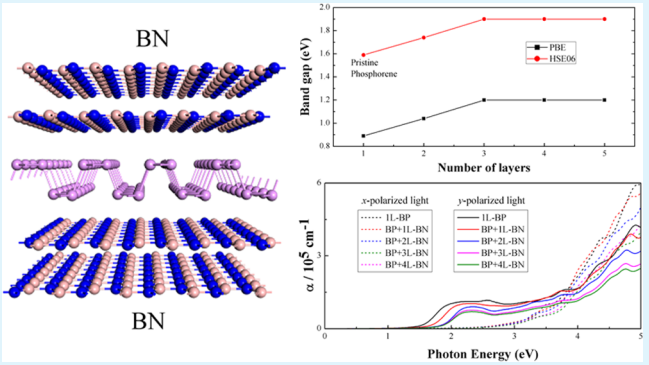

KEYWORDS: *phosphorene, heterostructure, band gap, anisotropic transport, optical property*

INTRODUCTION

The study of two-dimensional (2D) materials is now a rapidly growing research field in condensed matter physics and material sciences.[1] For instance, extensive studies have been performed on graphene,[2,3] hexagonal BN (h-BN),[4] MoS_2,[5] and other transition-metal dichalcogenides.[6] Recently, another 2D material, the so-called phosphorene, a monolayer of black phosphorus, has been introduced.[7,8] Each material has its own peculiar physical properties for various nanodevice applications. Among the various types of 2D materials, the phosphorene is receiving particular research interests because it has an intrinsic direct band gap at the Γ point. Besides, the few-layer phosphorene has a high carrier mobility of 300−1000 $cm^2 V^{-1} s^{-1}$.[8,9] This value is smaller than that in graphene, but the mobility of phosphorene is still higher than those of other 2D materials. In addition, the phosphorene shows anisotropic electrical[10] and optical properties regarding the zigzag and armchair directions.[11,12] Because of this large mobility, direct band gap, and anisotropic electrical and optical properties, the phosphorene may be superior to the graphene for various application purposes.

Despite the promising physical properties found in the phosphorene, it has been reported that the phosphorus has a trouble of degradation due to oxidation in ambient conditions.[13] Thus, it is an important issue to find a way to protect the intrinsic physical properties of phosphorene, and this can be achieved by capping or encapsulating the phosphorene layer. Usually, the 2D material has a weak van der Waals interlay interaction, and this makes it possible to obtain few-layers structures. Indeed, with the development of fabrication techniques, it is possible to artificially integrate dissimilar 2D members into a 2D heterostructure with a certain thickness and sequence of layers.[14,15] For instance, graphene/phosphorene bilayers,[16,17] p−n diode in phosphorene/MoS_2 heterojunction,[18] hybrid photocatalysts of phosphorene/TiO_2,[19] and phosphorene-based field-effect transistors with graphene/h-BN integrated[20] structures have been explored. By using these heterostructures, one may find diverse applications in more flexible ways. In this report, we choose the h-BN layers to protect phosphorene from degradation in the atmosphere.[20] Indeed, the air-stable h-BN-encapsulated phosphorene devices have been demonstrated.[21] However, a thorough study of the effect of the h-BN layer capping on phosphorene's properties is still lacking. In particular, the change in the intrinsic physical property of the phosphorene with different numbers of h-BN layers has not been investigated. This will be an important issue for electrical and optical device applications. Here, we explored the structural, electronic, and optical properties of the phosphorene monolayer (ML) on top of the one ML h-BN (bilayer heterostructure) and phosphorene monolayer encapsulated by the h-BN layers (sandwiched heterostructure). In the sandwiched systems, we changed the h-BN thickness and considered three types of structures: BN(1ML)/phosphorene/

Received: June 28, 2015
Accepted: October 6, 2015
Published: October 6, 2015

DOI: 10.1021/acsami.5b05694
ACS Appl. Mater. Interfaces 2015, 7, 23489−23495

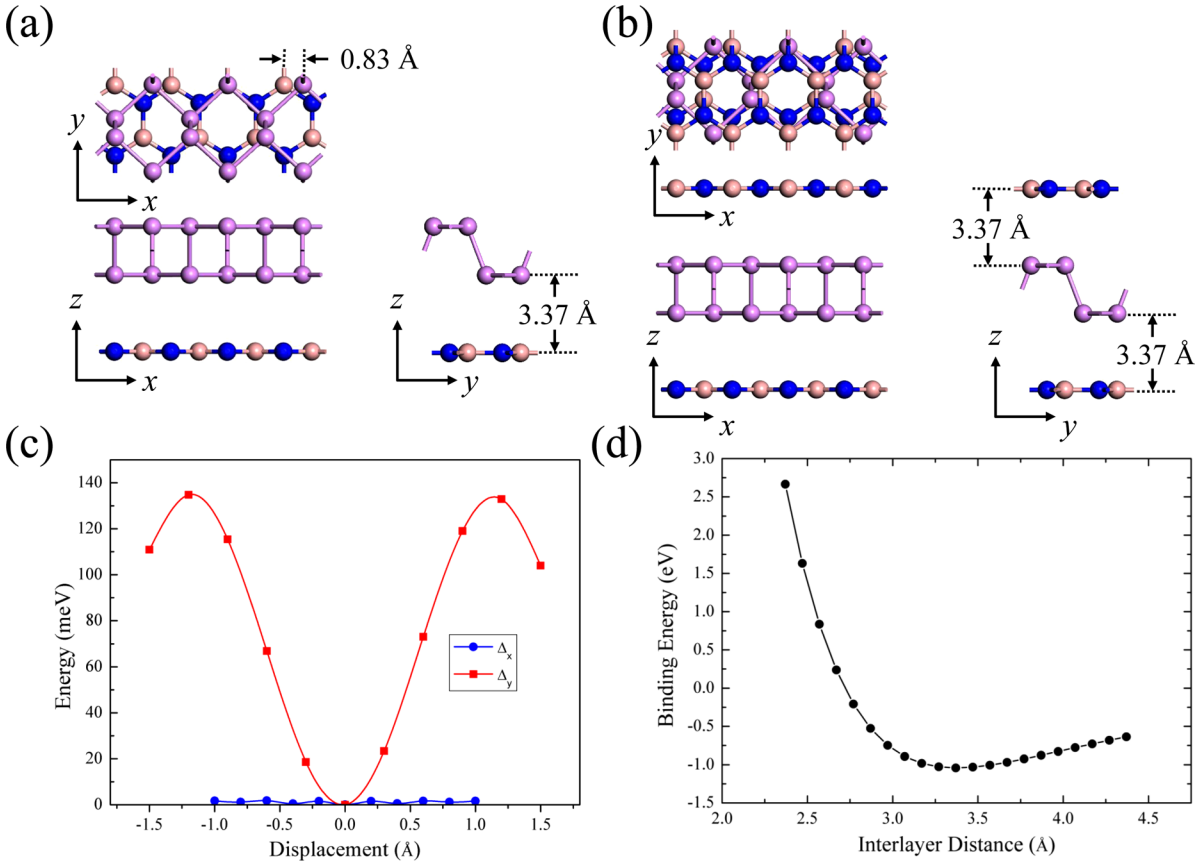

Figure 1. (a) Three basic orthographic views of the h-BN/phosphorene bilayer. 0.83 Å is the distance between the corresponding P and B atoms along the x direction. The interlayer distance is 3.37 Å. (b) Three basic orthographic views of the BN/phosphorene/BN trilayer. (c) Energy differences of a series of structures as a function of relative displacement in x (Δ_x) and y (Δ_y) directions. (d) Binding energy of BN/phosphorene bilayer as a function of the interlayer distance.

BN(1ML), BN(1ML)/phosphorene/BN(2ML), and BN-(2ML)/phosphorene/BN(2ML).

COMPUTATIONAL METHODS

We performed all the calculations using the Vienna *Ab initio* Simulation Package (VASP).[22,23] The generalized gradient approximation of Perdew–Burke–Ernzerhof (PBE) was employed.[24] Valence electrons were treated explicitly, and their interactions with ionic cores were described by projector augmented wave (PAW) pseudopotentials.[25] To describe the interlayer interaction of layer structured material, we included the van der Waals interaction of the optB88-vdW method.[26,27] We used the cutoff energy of 500 eV, and a vacuum region larger than 16 Å was applied. All the systems were fully optimized until the residual Hellmann–Feynman force on each atom was smaller than 0.01 eV/Å. The Brillouin zone integration was performed using the Monkhorst–Pack k-point sampling with a 3 × 7 k-mesh. We used the HSE06 hybrid functional[28,29] to calculate the band structures and optical properties. Concerning the modeling of our systems, the bilayer heterostructure was composed of one phosphorene layer and one h-BN layer, whereas the sandwiched heterostructure consisted of one phosphorene layer encapsulated by the h-BN layers. To resolve the lattice mismatch of the heterostructures, we chose a (3 × 1) primitive cell of a phosphorene layer and a (4 × 1) primitive orthorhombic cell of an h-BN layer. The lattice constant of the newly composed cell was chosen to fit to that of the 3 × 1 phosphorene cell. Thus, the lattice constants of the heterostructures were a = 9.90 Å (zigzag direction) and b = 4.62 Å (armchair direction), and this caused an overall strain of ∼1% .

RESULTS AND DISCUSSION

Figure 1a,b shows the three basic orthographic views of the optimized geometry of bilayer and sandwiched trilayer heterostructures. To obtain the most stable adsorption configuration in the bilayer structure, we started the relaxation of the composed structure from several initial positions of the phosphorene layer relative to the fixed h-BN layer. For the bilayer system, Figure 1a was the most stable adsorption configuration in the bilayer structure. To confirm this, we calculated the total energy by moving the phosphorene layer with respect to the h-BN layer by consecutive finite displacements along the x and y directions. Figure 1c shows the evolution of the total energy difference as a function of the in-plane displacement. The total energy in Figure 1a configuration was set to zero as a reference. We observed no meaningful energy difference (less than 2 meV) when we moved the phosphorene layer along the x direction (zigzag direction), thus it behaved like a frictionless motion. However, the energy difference was clearly pronounced along the y direction (armchair direction). For vertical movements, we calculated the total energy variation in Figure 1d, and the total energy minimum was achieved at an interlayer distance of 3.37 Å. Consequently, we found that Figure 1a was the true total energy minimum. Nonetheless, the energy difference was just about in the 0.1 eV regime when we displaced the phosphorene to the y direction up to 1 Å. This may imply that the phosphorene layer can be trapped in a position different from the lowest energy adsorption site in the growth process at finite

DOI: 10.1021/acsami.5b05694
ACS Appl. Mater. Interfaces 2015, 7, 23489–23495

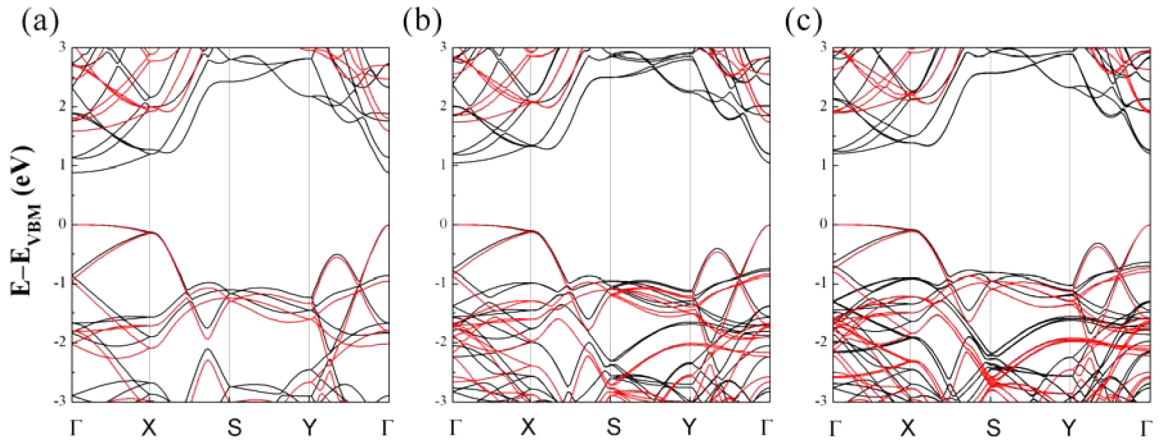

Figure 2. Calculated band structures of (a) pristine monolayer phosphorene, (b) BN/phosphorene bilayer, and (c) BN/phosphorene/BN trilayer. The black and red curves stand for PBE and HSE06 results, respectively.

temperatures. Indeed, we calculated the band structures in several other geometries and found no significant change as compared with that of the equilibrium geometry.

With the equilibrium adsorption structure shown in Figure 1a, we calculated the binding energy between the h-BN sheet and the phosphorene using the relation $E_b = [E_{p/BN} - (E_p + E_{BN})]$. Here, $E_{p/BN}$, E_p, and E_{BN} denote the total energy of the bilayer heterostructure, isolated single-layer phosphorene, and isolated h-BN layer. Since the h-BN layer has a total number of 16 atoms including both N and B atoms, the binding energy of the bilayer per atom of h-BN became 65 meV at the equilibrium distance. For the trilayer, the same magnitude of binding energy was achieved. Moreover, we found similar values of binding energies in thicker films. This value of binding energy has the same order of magnitude as observed in other van der Waals crystals such as graphite,[30] graphene/phosphorene heterostructures,[16] and bulk hexagonal boron nitride.[31] Indeed, we found no significant interlayer covalent bonding. Besides, the bond length and bond angle in the phosphorene/BN hybridized system were almost the same as those observed in an isolated individual layer. In addition, the in-plane electron density was very weakly redistributed in the hybridized system. Thus, we suggest that the phosphorene and h-BN layers are weakly bound by van der Waals interactions.

Figure 2a–c shows the calculated band structures of pristine phosphorene, bilayer, and trilayer systems, respectively. For an isolated phosphorene layer, the band gap was 0.89 eV with PBE and it became 1.59 eV with the hybrid functional method (HSE06). In general, the hybrid functional approach enhances the band gap by 0.7–0.8 eV as compared with the gap found using a PBE method in the phosphorene system. Our calculated band gap for a single layer phosphorene agreed with previous work.[32] In the bilayer heterostructure, we found a direct energy band gap of 1.04 and 1.74 eV using PBE and hybrid functional methods, respectively. Thus, the h-BN substrate contributed to enhancing the band gap by 0.15 eV. Nonetheless, the spectral shapes of the band structure near the conduction band minimum (CBM) and valence band maximum (VBM) were almost the same as that of an isolated phosphorene layer. Therefore, the electrical transport behavior of the bilayer heterostructure will be still governed by the phosphorene. In the trilayer heterostructure, the band gap was further enhanced to 1.20 and 1.90 eV with PBE and HSE06 methods, respectively. Even with the enhanced gap, the general band shapes were preserved again. This will be a very important feature for phosphorene-based device applications because the h-BN layers not only protect the phosphorene from degradation in ambient conditions but also do not significantly disturb the intrinsic electronic structure of phosphorene. We found that the band gap of the phosphorene layer was enhanced due to the h-BN layer and each h-BN layer contributed to enhancing the band gap of ∼0.15 eV. For the two thicker systems such as BN(1ML)/phosphorene/BN(2ML) and BN(2ML)/phosphorene/BN(2ML), we found a band gap of 1.90 eV with the HSE06 method. Thus, the band gap found in the BN(1ML)/phosphorene/BN(1ML) structure was a saturated value. The spectral shapes of the band structure of these two systems were also most the same as that of BN(1ML)/phosphorene/BN(1ML). This result indicates that the BN(1ML)/phosphorene/BN(1ML) is well-protected and another h-BN adlayer does not affect the fundamental property of the phosphorene layer. As a result, we propose that only the interface layer contributes to enhancing the band gap, and this is a very important phenomenon for device application. Figure 3 shows the calculated density of states (DOS) of the pristine phosphorene layer, isolated h-BN, phosphorene/BN(1ML), and BN(1ML)/phosphorene/BN(1ML) systems. As shown in the PDOS of the heterostructures, the phosphorus atom mostly contributed to the low-lying bands near the CBM and VBM. In particular, the low-lying valence band mostly consisted of the phosphorus p_z orbital. By analyzing the total DOS in Figure 3a, we found that the peak positions of the heterostructures in the conduction band shifted to a higher energy region slightly comparing to the isolated phosphorene. This results in an enhancement of the band gap. Moreover, from the perspective of elementary quantum mechanics, it is well-known that, if two levels are interacting with each other, then the level spacing is increased due to this interaction. In our hybridized structure, both phosphorene and h-BN layers are coupled by a weak van der Waals interaction. Thus, in a qualitative manner, we can understand the band gap enhancement affected by the h-BN layer.

It has been known that the phosphorene has an anisotropic electrical transport property. Thus, it will be an important issue to explore how the effective mass and anisotropic property are affected by the h-BN layer. To reveal this, we estimated the effective mass from the calculated band structures using the HSE06 method. Here, for the effective mass estimation, we

DOI: 10.1021/acsami.5b05694
ACS Appl. Mater. Interfaces 2015, 7, 23489–23495

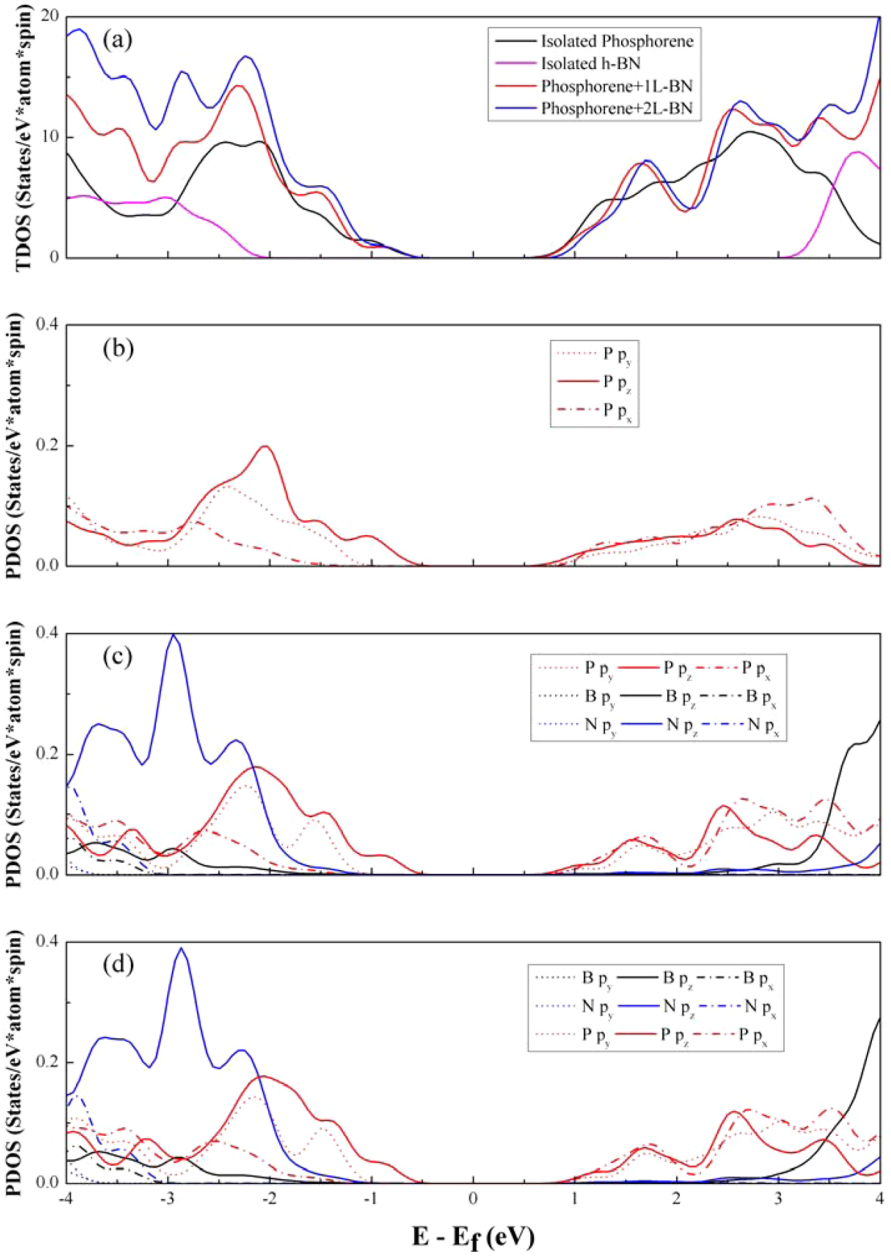

Figure 3. (a) Calculated (HSE06 method) total density of states (TDOS) of isolated phosphorene, isolated h-BN, BN/phosphorene bilayer, and BN/phosphorene/BN trilayer systems. Calculated projected density of states (PDOS) of (b) pristine monolayer phosphorene, (c) BN/phosphorene bilayer, and (d) BN/phosphorene/BN trilayer.

assume quadratic band dispersion near the CBM and VBM. The calculated results are presented in Table 1. For the pristine phosphorene, the hole and electron carrier effective masses along the Γ−X direction (zigzag direction) are much heavier than those along the Γ−Y direction (armchair direction), and our estimated effective masses are quite close to the previous result.[12] In heterostructures, we observed that the effective mass in conduction and valence bands was increased due to the capping of the BN layer. As shown in Figure 2, the band dispersion along the Γ−Y direction shows a well-behaved quadratic feature, but the band dispersion of VBM deviates from a nice quadratic feature along the Γ−X direction. This may cause a small numerical error in the estimation of a very accurate hole effective mass. Nonetheless, we observe an interesting characteristic. In the heterostructure, despite a small suppression in the anisotropic ratio, the most essential finding is that the anisotropic effective mass is still preserved even in the presence of BN layers. This may imply that the intrinsic

Table 1. Calculated Ratio of Effective Mass of Hole (m_h^*/m_e) and Electron (m_e^*/m_e) in the Pristine Phosphorene and the Heterostructures[a]

	Γ−X		Γ−Y	
	(m_h^*/m_e)	(m_e^*/m_e)	(m_h^*/m_e)	(m_e^*/m_e)
bare phosphorene	7.43	1.20	0.17	0.19
BP+1L-BN	7.49	1.24	0.20	0.21
BP+2L-BN	8.5	1.25	0.23	0.23
BP+3L-BN	8.53	1.25	0.23	0.23
BP+4L-BN	8.67	1.25	0.23	0.23

[a]The m_e is the electron rest mass.

DOI: 10.1021/acsami.5b05694
ACS Appl. Mater. Interfaces 2015, 7, 23489−23495

anisotropic electrical transport property observed in the pristine layer can be maintained in the BN/phosphorene/BN systems.

Along with the anisotropic transport property, the phosphorene layer also displays an anisotropic optical property. Thus, we calculated the optical properties. Here, we considered two electric field polarizations such as zigzag and armchair directions. In general, the optical property of a material can be understood from the frequency-dependent dielectric function $\epsilon(\omega) = \varepsilon_1(\omega) + i\varepsilon_2(\omega)$. Figure 4 shows the frequency-dependent dielectric functions along armchair and zigzag directions using the HSE06 functional method. We only show the imaginary part of the dielectric function because the real part can be extracted from the Kramers−Kronig relation. For the electric field polarization along the armchair direction, the first peak position in the pristine phosphorene layer was observed at ∼1.5 eV. Interestingly, the first peak positions moved to 1.65 and 1.8 eV in the bilayer and trilayer systems, respectively. Beyond the trilayer thickness, we observed no significant change in the peak positions. Thus, we clearly found a blue shift in the first peak position as the film thickness increased because it moved to a high energy regime. This behavior can be understood from the calculated band structure shown in Figure 2 because the CBM near the Γ−Y direction shows an upward shift as the film thickness increases. Consequently, we observed a blue shift characteristic. For the electric field polarization along the zigzag direction, the first peak position in the pristine phosphorene layer was observed at ∼3.1 eV. However, we observed a red shift characteristic in the peak position as the film thickness increased. In this case, we were not able to find proper optical transition levels corresponding to 3.1 eV from the band structure along the high symmetry directions. This may imply that the optical transition between the valence band and conduction bands for the electric field polarization along the zigzag direction occurs in another region of the Brillouin zone. Indeed, the similar behavior has been shown in a few-layer black phosphorus structure.[12] Comparing the dielectric functions between these two different electric polarizations, we find that the h-BN has an opposite effect on the phosphorene's optical property along armchair and zigzag directions. The position of the absorption peak is blue-shifted to 1.82 eV with two h-BN layers for armchair polarized light, and no more increasing with more h-BN layers. For zigzag polarized light, the position is gradually red-shifted to 2.79 eV with increasing number of h-BN layers. The anisotropic optical property of phosphorene is still preserved even in the presence of a few layers of h-BN. From the calculated frequency-dependent dielectric function, we also calculated the absorption coefficient $\alpha(E) = (4\pi E/hc)\{[(\varepsilon_1^2 + \varepsilon_2^2)^{1/2} - \varepsilon_1]/2\}^{1/2}$, where E is the energy of the incident light. Figure 5 shows the calculated results. As expected from the calculated frequency-dependent dielectric functions, the frequency-dependent absorption coefficients displayed the same anisotropic behavior. Overall, we find that the intrinsic anisotropic optical property of the phosphorene layer is still maintained in BN/phosphorene/BN heterostructures.

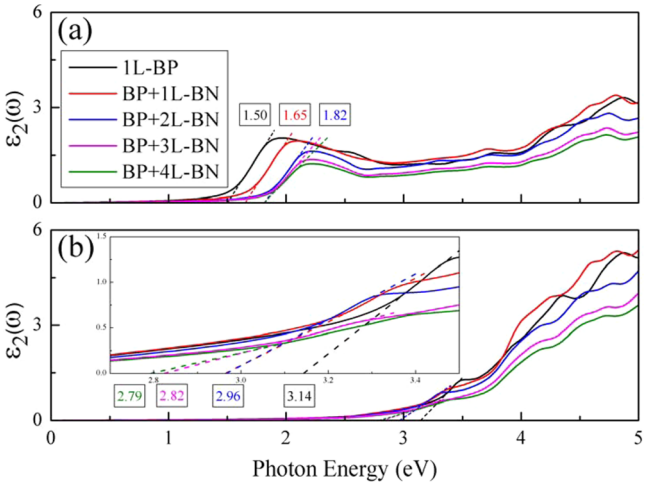

Figure 4. Imaginary part of frequency-dependent dielectric function in phosphorene monolayer and the heterostructures for the incident light polarized along the (a) armchair (y) direction and (b) zigzag (x) direction. The dashed lines are tangent lines of the first absorption peak; they provide the positions of band edges for the corresponding cases. The extrapolated values are shown in the small boxes. The inset in (b) is a zoom-in figure with an energy range from 2.7 to 3.5 eV. For the armchair polarized incident light, the positions of band edges are 1.50, 1.65, 1.82, 1.82, and 1.82 eV for the cases of isolated phosphorene, phosphorene/BN(1ML), BN(1ML)/phosphorene/BN(1ML), BN(1ML)/phosphorene/BN(2ML), and BN(2ML)/phosphorene/BN(2ML) systems, respectively. For the zigzag polarized incident light, the positions of the corresponding systems are 3.14, 2.96, 2.96, 2.82, and 2.79 eV.

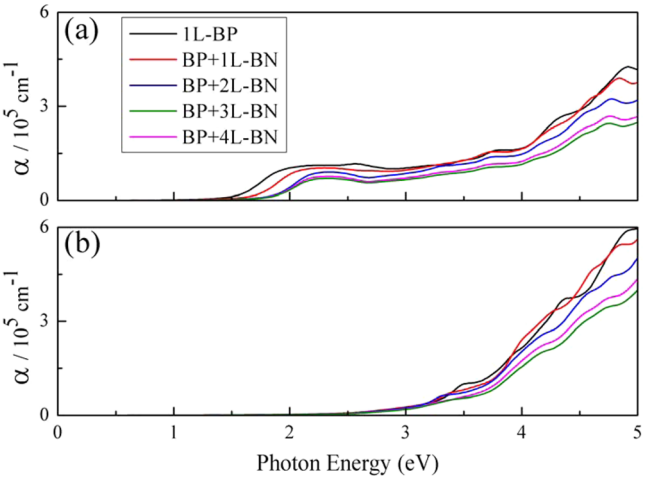

Figure 5. Optical absorption spectra of phosphorene monolayer and the heterostructures for the incident light polarized along the (a) armchair (y) direction and (b) zigzag (x) direction.

CONCLUSION

In summary, we systematically studied the electronic and optical properties of heterostructures consisting of phosphorene and the h-BN. We found that the interlayer distance and the binding energy of the heterostructures were similar to those of other van der Waals crystals. The band gap of the isolated phosphorene was about 1.59 eV with the HSE06 method. Interestingly, the h-BN layer contributed to enhancing the band gap. For instance, the calculated band gap in the phosphorene/BN bilayer was 1.74 eV, and it became 1.9 eV in BN(1ML)/phosphorene/BN(1ML). However, the band gap found in the BN(1ML)/phosphorene/BN(1ML) system was a saturated value because the band gap was not further enhanced when we continuously increased the thickness of h-BN layers even up to four layers (two bottom and two top layers). We observed that both hole and electron effective masses were slightly increased

DOI: 10.1021/acsami.5b05694
ACS Appl. Mater. Interfaces 2015, 7, 23489−23495

with the increasing h-BN thickness. Despite this h-BN thickness-dependent characteristic, the anisotropic effective mass was still maintained in the heterostructures. In addition, we found a blue shift in the peak positions of the dielectric function and optical absorption coefficient for the electric field polarization along the armchair direction, whereas a red shift was observed for the electric field polarization along the zigzag direction. Nonetheless, the optical anisotropy was still preserved. Overall, we find that the intrinsic physical properties of the pristine phosphorene layer are not strongly disturbed by adding the h-BN layers. This feature suggests that the h-BN layers can be a good candidate to protect the phosphorene layer from its degradation in ambient conditions and the heterostructure can be utilized for phosphorene-based optoelectronic device applications.

AUTHOR INFORMATION

Corresponding Author

*E-mail: hongj@pknu.ac.kr.

Notes

The authors declare no competing financial interest.

ACKNOWLEDGMENTS

This research was supported by the Basic Science Research Program through the National Research Foundation of Korea (NRF) funded by the Ministry of Education, Science and Technology (No. 2013R1A1A2006071) and by the Supercomputing Center/Korea Institute of Science and Technology Information with supercomputing resources including technical support (KSC-2015-C3-040).

REFERENCES

(1) Butler, S. Z.; Hollen, S. M.; Cao, L.; Cui, Y.; Gupta, J. A.; Gutiérrez, H. R.; Heinz, T. F.; Hong, S. S.; Huang, J.; Ismach, A. F.; Johnston-Halperin, E.; Kuno, M.; Plashnitsa, V. V.; Robinson, R. D.; Ruoff, R. S.; Salahuddin, S.; Shan, J.; Shi, L.; Spencer, M. G.; Terrones, M.; Windl, W.; Goldberger, J. E. Progress, Challenges, and Opportunities in Two-Dimensional Materials Beyond Graphene. *ACS Nano* **2013**, *7*, 2898−2926.

(2) Novoselov, K. S.; Geim, A. K.; Morozov, S. V.; Jiang, D.; Zhang, Y.; Dubonos, S. V.; Grigorieva, I. V.; Firsov, A. A. Electric Field Effect in Atomically Thin Carbon Films. *Science* **2004**, *306*, 666−669.

(3) Geim, A. K.; Novoselov, K. S. The Rise of Graphene. *Nat. Mater.* **2007**, *6*, 183−191.

(4) Pakdel, A.; Bando, Y.; Golberg, D. Nano Boron Nitride Flatland. *Chem. Soc. Rev.* **2014**, *43* (3), 934−959.

(5) Ganatra, R.; Zhang, Q. Few-Layer MoS2: A Promising Layered Semiconductor. *ACS Nano* **2014**, *8*, 4074−4099.

(6) Wang, Q. H.; Kalantar-Zadeh, K.; Kis, A.; Coleman, J. N.; Strano, M. S. Electronics and Optoelectronics of Two-Dimensional Transition Metal Dichalcogenides. *Nat. Nanotechnol.* **2012**, *7*, 699−712.

(7) Li, L.; Yu, Y.; Ye, G. J.; Ge, Q.; Ou, X.; Wu, H.; Feng, D.; Chen, X. H.; Zhang, Y. Black Phosphorus Field-Effect Transistors. *Nat. Nanotechnol.* **2014**, *9*, 372−377.

(8) Liu, H.; Neal, A. T.; Zhu, Z.; Luo, Z.; Xu, X.; Tománek, D.; Ye, P. D. Phosphorene: An Unexplored 2D Semiconductor with a High Hole Mobility. *ACS Nano* **2014**, *8*, 4033−4041.

(9) Xia, F.; Wang, H.; Jia, Y. Rediscovering Black Phosphorus as an Anisotropic Layered Material for Optoelectronics and Electronics. *Nat. Commun.* **2014**, *5*, 4458.

(10) Fei, R.; Yang, L. Strain-Engineering the Anisotropic Electrical Conductance of Few-Layer Black Phosphorus. *Nano Lett.* **2014**, *14*, 2884−2889.

(11) Tran, V.; Soklaski, R.; Liang, Y.; Yang, L. Layer-Controlled Band Gap and Anisotropic Excitons in Few-Layer Black Phosphorus. *Phys. Rev. B: Condens. Matter Mater. Phys.* **2014**, *89*, 235319.

(12) Qiao, J.; Kong, X.; Hu, Z.-X.; Yang, F.; Ji, W. High-Mobility Transport Anisotropy and Linear Dichroism in Few-Layer Black Phosphorus. *Nat. Commun.* **2014**, *5*, 4475.

(13) Island, J. O.; Steele, G. A.; van der Zant, H. S. J.; Castellanos-Gomez, A. Environmental Instability of Few-Layer Black Phosphorus. *2D Mater.* **2015**, *2*, 011002.

(14) Geim, A. K.; Grigorieva, I. V. Van Der Waals Heterostructures. *Nature* **2013**, *499*, 419−425.

(15) Wang, H.; Liu, F.; Fu, W.; Fang, Z.; Zhou, W.; Liu, Z. Two-Dimensional Heterostructures: Fabrication, Characterization, and Application. *Nanoscale* **2014**, *6*, 12250−12272.

(16) Padilha, J. E.; Fazzio, A.; da Silva, A. J. R. van Der Waals Heterostructure of Phosphorene and Graphene: Tuning the Schottky Barrier and Doping by Electrostatic Gating. *Phys. Rev. Lett.* **2015**, *114*, 066803.

(17) Hu, W.; Wang, T.; Yang, J. Tunable Schottky Contacts in Hybrid Graphene−phosphorene Nanocomposites. *J. Mater. Chem. C* **2015**, *3*, 4756−4761.

(18) Deng, Y.; Luo, Z.; Conrad, N. J.; Liu, H.; Gong, Y.; Najmaei, S.; Ajayan, P. M.; Lou, J.; Xu, X.; Ye, P. D. Black Phosphorus−Monolayer MoS2 van Der Waals Heterojunction P−n Diode. *ACS Nano* **2014**, *8*, 8292−8299.

(19) Uk Lee, H.; Lee, S. C.; Won, J.; Son, B.-C.; Choi, S.; Kim, Y.; Park, S. Y.; Kim, H.-S.; Lee, Y.-C.; Lee, J. Stable Semiconductor Black Phosphorus (BP)@titanium Dioxide (TiO2) Hybrid Photocatalysts. *Sci. Rep.* **2015**, *5*, 8691.

(20) Avsar, A.; Vera-Marun, I. J.; Tan, J. Y.; Watanabe, K.; Taniguchi, T.; Castro Neto, A. H.; Özyilmaz, B. Air-Stable Transport in Graphene-Contacted, Fully Encapsulated Ultrathin Black Phosphorus-Based Field-Effect Transistors. *ACS Nano* **2015**, *9*, 4138−4145.

(21) Gillgren, N.; Wickramaratne, D.; Shi, Y.; Espiritu, T.; Yang, J.; Hu, J.; Wei, J.; Liu, X.; Mao, Z.; Watanabe, K.; Taniguchi, T.; Bockrath, M.; Barlas, Y.; Lake, R. K.; Lau, C. N. Gate Tunable Quantum Oscillations in Air-Stable and High Mobility Few-Layer Phosphorene Heterostructures. *2D Mater.* **2015**, *2*, 011001.

(22) Kresse, G.; Furthmüller, J. Efficiency of Ab-Initio Total Energy Calculations for Metals and Semiconductors Using a Plane-Wave Basis Set. *Comput. Mater. Sci.* **1996**, *6*, 15−50.

(23) Kresse, G.; Furthmüller, J. Efficient Iterative Schemes for Ab Initio Total-Energy Calculations Using a Plane-Wave Basis Set. *Phys. Rev. B: Condens. Matter Mater. Phys.* **1996**, *54*, 11169−11186.

(24) Perdew, J. P.; Burke, K.; Ernzerhof, M. Generalized Gradient Approximation Made Simple. *Phys. Rev. Lett.* **1996**, *77*, 3865−3868.

(25) Kresse, G.; Joubert, D. From Ultrasoft Pseudopotentials to the Projector Augmented-Wave Method. *Phys. Rev. B: Condens. Matter Mater. Phys.* **1999**, *59*, 1758−1775.

(26) Klimeš, J.; Bowler, D. R.; Michaelides, A. Chemical Accuracy for the van Der Waals Density Functional. *J. Phys.: Condens. Matter* **2010**, *22*, 022201−022205.

(27) Klimeš, J.; Bowler, D. R.; Michaelides, A. Van Der Waals Density Functionals Applied to Solids. *Phys. Rev. B: Condens. Matter Mater. Phys.* **2011**, *83*, 195131−195143.

(28) Heyd, J.; Scuseria, G. E.; Ernzerhof, M. Hybrid Functionals Based on a Screened Coulomb Potential. *J. Chem. Phys.* **2003**, *118*, 8207−8215.

(29) Heyd, J.; Scuseria, G. E.; Ernzerhof, M. Erratum: "Hybrid Functionals Based on a Screened Coulomb Potential" [J. Chem. Phys.118, 8207 (2003)]. *J. Chem. Phys.* **2006**, *124*, 219906.

(30) Chakarova-Käck, S. D.; Schröder, E.; Lundqvist, B. I.; Langreth, D. C. Application of van Der Waals Density Functional to an Extended System: Adsorption of Benzene and Naphthalene on Graphite. *Phys. Rev. Lett.* **2006**, *96*, 146107.

(31) Graziano, G.; Klimeš, J.; Fernandez-Alonso, F.; Michaelides, A. Improved Description of Soft Layered Materials with van Der Waals Density Functional Theory. *J. Phys.: Condens. Matter* **2012**, *24*, 424216.

DOI: 10.1021/acsami.5b05694
ACS Appl. Mater. Interfaces 2015, 7, 23489−23495

(32) Han, X.; Morgan Stewart, H.; Shevlin, S. A.; Catlow, C. R. A.; Guo, Z. X. Strain and Orientation Modulated Bandgaps and Effective Masses of Phosphorene Nanoribbons. *Nano Lett.* **2014**, *14*, 4607−4614.

DOI: 10.1021/acsami.5b05694
ACS Appl. Mater. Interfaces 2015, 7, 23489−23495